Molecular Biology of the Cell
Vol. 15, 2253–2263, May 2004

Uncoated Endocytic Vesicles Require the Unconventional Myosin, Myo6, for Rapid Transport through Actin Barriers[D][V]

Laura Aschenbrenner, Samia N. Naccache, and Tama Hasson*

Section of Cell and Developmental Biology, Division of Biological Sciences, University of California at San Diego, La Jolla, California 92093

Submitted January 4, 2004; Revised February 19, 2004; Accepted February 23, 2004
Monitoring Editor: Anthony Bretscher

After clathrin-mediated endocytosis, clathrin removal yields an uncoated vesicle population primed for fusion with the early endosome. Here we present the first characterization of uncoated vesicles and show that myo6, an unconventional myosin, functions to move these vesicles out of actin-rich regions found in epithelial cells. Time-lapse microscopy revealed that myo6-associated uncoated vesicles were motile and exhibited fusion and stretching events before endosome delivery, processes that were dependent on myo6 motor activity. In the absence of myo6 motor activity, uncoated vesicles remained trapped in the actin mesh, where they exhibited Brownian-like motion. Exit from the actin mesh occurred by a slow diffusion-based mechanism, delaying transferrin trafficking to the early endosome. Expression of a myo6 mutant that bound tightly to F-actin produced immobilized vesicles and blocked trafficking. Depolymerization of the actin cytoskeleton rescued this block and specifically accelerated transferrin delivery to the early endosome without affecting earlier steps in endocytosis. Therefore actin is a physical barrier impeding uncoated vesicle trafficking, and myo6 is recruited to move the vesicles through this barrier for fusion with the early endosome.

INTRODUCTION

Clathrin-dependent receptor-mediated endocytosis is a multistep process resulting in the delivery of internalized ligand-receptor complexes to the early endosome. The first step is clathrin-coated vesicle formation, a process that requires the action of a growing array of accessory proteins and the GTPase, dynamin (reviewed in Schmid, 1997). After clathrin uncoating, Rab5, a series of Rab5 effectors, and PI3-kinase are recruited to facilitate early endosome antigen 1 (EEA1)-mediated docking and uncoated vesicle fusion with the early endosome (reviewed in Clague, 1998; Gruenberg, 2001). Although these budding and fusion processes have been well characterized, the mechanism whereby the short-lived uncoated vesicles are transported to the early endosomes for fusion has received less attention.

Both clathrin-coated vesicle formation and uncoating occur immediately under the plasma membrane, where there is a cortical actin cytoskeletal layer. Cortical actin filaments are polarized with their plus ends at the plasma membrane and their minus ends facing inward and are further cross-linked into a meshwork by actin-binding proteins such as spectrin and myosin II. In many cell types, the actin meshwork is sufficiently dense that it was predicted to be a barrier to transport of the recently uncoated endocytic vesicles toward the more centrally located early endosome (reviewed in Qualmann *et al.*, 2000; Qualmann and Kessels, 2002; Hasson, 2003). However, it had not been possible to test this hypothesis directly because of the lack of a specific uncoated vesicle marker.

Recently, an actin-based molecular motor, the unconventional myosin myo6 has been shown to associate with uncoated vesicles (Aschenbrenner *et al.*, 2003). Unlike other myosins, myo6 travels toward the minus end of actin filaments (Wells *et al.*, 1999). This directionality of movement suggests that, if the actin cortex were a barrier to uncoated vesicle trafficking, then myo6 could be used to overcome it. Myo6 has three structural domains: an N-terminal conserved motor domain which binds a single calmodulin light chain, a coiled-coil region that mediates dimerization, and a C-terminal globular domain that is the cargo-binding domain. This globular tail targets myo6 to uncoated endocytic vesicles (Aschenbrenner *et al.*, 2003).

Overexpression of the globular tail domain of myo6 displaces the endogenous myo6 from uncoated vesicles and delays transferrin trafficking to the early endosome due to an accumulation of uncoated vesicles in actin-rich cell peripheries (Aschenbrenner *et al.*, 2003). These vesicles lacked EEA1, suggesting that they were en route to the early endosome but had not yet fused with it. The vesicles appeared competent for fusion, however, because they had recruited the fusion factor Rab5 (Aschenbrenner *et al.*, 2003). These studies suggested that myo6 could be an accessory protein recruited to the nascent uncoated endocytic vesicles to move them out of the actin-rich cell peripheries or, alternatively, that myo6 could be a regulator of uncoated vesicle fusion with the early endosome.

Here we directly test myo6's roles in vesicle trafficking by characterizing the motile properties of uncoated vesicles using GFP-tagged versions of myo6 as markers. We also test the importance of F-actin in vesicle trafficking. We conclude that actin is a barrier to inward endocytic vesicle movement

Article published online ahead of print. Mol. Biol. Cell 10.1091/mbc.E04–01–0002. Article and publication date are available at www.molbiolcell.org/cgi/doi/10.1091/mbc.E04–01–0002.

[D][V] Online version of this article contains supporting material. Online version is available at www.molbiolcell.org.

* Corresponding author. E-mail address: tama@ucsd.edu.

and that myo6 is specifically recruited to the vesicle surface to move vesicles through this barrier.

MATERIALS AND METHODS

Cell Culture and Transfection

ARPE-19 cells (Dunn *et al.*, 1996) were grown at 37°C with 5% CO_2 in DMEM-F12 with 10% FBS, fungizone, and glutamine and transfected with GFP-tagged myo6 constructs as described (Aschenbrenner *et al.*, 2003).

Antibodies

Antibodies used in this study were from the following sources: BD Transduction Laboratories (Lexington, KY): anticlathrin heavy chain, anti-EEA1; Sigma (St. Louis, MO): anti-human transferrin receptor (CD71); and Jackson ImmunoResearch Laboratories (West Grove, PA): FITC- and rhodamine-conjugated donkey anti-rabbit and anti-mouse antibodies. All were used at concentrations the manufacturer recommended. Antibody to the clathrin adapter AP-2 was generously provided by Dr. Sandra Schmid (The Scripps Research Institute, La Jolla, CA). Affinity-purified rabbit anti-myo6 tail domain antibodies were as described (Hasson and Mooseker, 1994).

Myo6 GFP Constructs

The Quick Change XL site directed mutagenesis kit (Stratagene, La Jolla, CA) was used to generate the myo6 motor domain mutant. GFP-M6(K157R) was created from GFP-M6 (Aschenbrenner *et al.*, 2003) using the primers p6-K157R-sense (5′-caggagctggcagaacggaaaatac) and p6-K157R-antisense (5′-gtattttccgttctgccagctcctg). The mutation in the primer set is underlined. Isolated clones were sequenced to verify that the point mutation was incorporated and that no other mutations were introduced by PCR.

Immunofluorescence and Time-lapse Video Microscopy

Coverslip grown cells were processed for immunofluorescence in six-well plates as described (Hasson and Mooseker, 1994). All fixed samples were observed with a Leica DMR upright light microscope (Deerfield, IL) fitted with a Hamamatsu ORCA 10-bit CCD digital camera (Bridgewater, NJ) as described (Aschenbrenner *et al.*, 2003).

The movement of GFP-labeled vesicles in ARPE-19 cells was monitored at 25°C using the Leica DMR fitted with a Plan Apochromat 100× 1.4 NA oil immersion objective. The transfected cells were mounted in a chamber in imaging medium consisting of DMEM-F12 lacking phenol red and containing 35 mM HEPES and 10% FBS. Illumination was provided by a halogen lamp with a green filter for phase-contrast observations, or a 50 W HBO mercury arc lamp for fluorescence. To visualize the GFP fluorescence, the following filters were used: excitation, BP 473/95, emission, BP 530/40. All images were captured using the ORCA camera controlled by Openlab 3.1.4 software (Improvision, Lexington, MA). Exposure times varied from 250-ms to 3.5-s exposure, depending on the GFP expression level. We found that a 10-s minimum between exposures was necessary to minimize cell distress and cell contraction. Therefore, images were captured at a rate of one frame every 15, 20, or 30 s depending on the exposure time and GFP-construct used. Openlab software was used to control both the switch between GFP fluorescence and phase contrast as well as the shutter limiting light exposure to the sample. All cells were monitored for a minimum of 13 min, and cell health was checked by phase-contrast microscopy. Any cells exhibiting contraction were eliminated from the analysis.

Image Analysis

The position of distinct vesicles that were initially positioned within 10 μm of the cell edge was manually determined in successive frames using Openlab measurements software. Two hundred fifty vesicles present for a 40-s minimum (2 video frames) were tracked for each GFP-construct studied. Supplementary vesicle tracking was undertaken in GFP-M6–expressing cells to quantify the number of vesicles with <40-s lifetimes, determining that 98.3% of vesicles tracked were visible for 2 or more frames, whereas 1.6% was present for a single frame (lifetime: 0–39 s). Each construct was analyzed in 2–5 separate experiments, and 7 cells minimum per experiment were recorded. For each experiment tracking cells expressing a mutated version of myo6, a wild-type GFP-M6 control was also tracked to ensure cell health. The Openlab software recorded the (x,y) coordinates of the fluorescent particles at each given time, calculated vesicle trajectories, and calculated the instantaneous velocity ($\Delta d/\Delta t$). The displacement vector analysis, representing the distance covered from the initial point of vesicle appearance to the final point before disappearance, was plotted using Canvas 6.0 utilizing the x,y coordinates. Plots and statistical analyses of vesicle properties were generated with Microsoft Excel 2000 (Redmond, WA).

To quantify vesicle stretching and fusion events, all vesicles present in 250-μm^2 areas from two different transfected cells were monitored for more than eight nonoverlapping 1-min time periods (~30 distinct vesicles at any one time point; >180 vesicles). In GFP-M6tail- and GFP-M6(K157R)–expressing cells, this analysis was extended to 500 μm^2 for the length of the movie to monitor a statistically significant number of events.

Two-dimensional diffusion coefficients were calculated by plotting the mean square displacement vs. the time interval as described by Abney *et al.* (1999) using the equation $\langle d^2(t)\rangle = 4Dt + v^2t^2$. Here d is the displacement, t the time, D the diffusion coefficient, and v the vesicle velocity. We assumed velocity to be constant as no active myo6 motor was associated with the vesicles analyzed. Only vesicles exhibiting a linear plot (coefficient of determination >0.90) were used to calculate D.

Steady State Uptake Assay for Endocytosis

Steady state uptakes were undertaken and quantified as described (Aschenbrenner *et al.*, 2003). In some experiments after serum starvation cells were further incubated for 30 min at 37°C in serum-free DMEM-F12 medium containing 0.015 μM latrunculin A (DMEM-F12/LatA; LatA was purchased from Biomol [Plymouth Meeting, PA] or Calbiochem [San Diego, CA] or its solvent dimethylsulfoxide (DMEM-F12/DMSO). After starvation, the medium was replaced with DMEM-F12 containing 25 μg/ml rhodamine-conjugated transferrin (R-Tsfn; Molecular Probes, Eugene, OR), and uptake was allowed to proceed at 37°C for 1–30 min.

Pulse-chase Uptake of R-Tsfn

Pulse-chase uptakes were undertaken as described (Aschenbrenner *et al.*, 2003). For pulse-chase experiments in the presence of DMSO or LatA, following 1.5-h serum starvation, the cells were incubated for 30 min in DMEM-F12/LatA or DMEM-F12/DMSO at 37°C. The cells were then incubated on ice for 30 min in the appropriate media before an additional 1 h on ice with 25 μg/ml R-Tsfn in DMEM-F12/LatA or DMEM-F12/DMSO media. Cells were washed at 4°C with DMEM-F12 to remove unbound transferrin, before transferring to 37°C for 1–30 min to allow uptake to proceed.

Quantification of Trafficking Using Fluorescence

Quantification of steady state R-Tsfn uptake to the pericentriolar endosome and quantification of percent overlap between GFP-tagged constructs, R-Tsfn, and endocytic markers was done as described (Aschenbrenner *et al.*, 2003).

Published pulse-chase experiments in ARPE-19 cells have confirmed that after exit from the myo6-positive uncoated vesicle compartment, R-Tsfn enters peripheral early endosomes that are EEA1-positive (Aschenbrenner *et al.*, 2003). For experiments undertaken in the presence of DMSO or LatA, quantification of this delivery was accomplished by using the fact that given longer chase times in ARPE-19 cells, the EEA1-positive pericentriolar region receives the endocytosed transferrin. Of note, at these later pulse-chase time points, overlap between the endocytosed transferrin and myo6 is no longer seen confirming complete delivery of the transferrin to the early endosome compartment (Aschenbrenner *et al.*, 2003). Therefore to quantify delivery of transferrin from the uncoated vesicles to the early endosome in DMSO- or Lat A–treated cell, the cells were scored as positive for delivery to the early endosome if any pericentriolar R-Tsfn was evident. In some experiments, the position of the early endosome was confirmed by staining for EEA1 during quantification of early endosome delivery. Error bars represent the SD from three experiments.

Quantification of Transferrin Endocytosis Using an ELISA Assay

ARPE-19 cells were serum-starved as described above and incubated for an additional 30 min at 37°C in DMEM-F12/LatA or DMEM-F12/DMSO. The cells were chilled on ice for 20 min, and the medium was replaced with ice-cold DMEM-F12/LatA or DMEM-F12/DMSO containing 25 μg/ml human biotinylated transferrin (Sigma) and incubated on ice for an additional 1 h to label surface receptors. Cells were washed twice with 0.5% BSA in PBS at 4°C before placing the cells back at 37°C for 0–15 min with the appropriate DMEM-F12 medium.

To quantify transferrin endocytosis, transferrin still bound to the cell surface was stripped by washing twice for 30 s each with 10 mM HCl + 150 mM NaCl. Cells were then washed with PBS before removal from the culture dish using PBS containing 5 mM EDTA. Cells were lysed in PBS containing 1% TX-100, and protein concentrations were determined using a BCA assay (Pierce Chemical Co., Rockford, IL). The amount of transferrin taken up by each cell culture was quantified using an ELISA-based assay as described (Smythe *et al.*, 1992). A 1:10,000 dilution of rabbit antitransferrin antibody (United States Biological, Swampscott, MA) was used to coat the ELISA plates. Streptavidin-HRP (Molecular Probes) was used at 1 μg/ml. After color development, the absorbance at 492 nm read using a Versamax tunable microplate reader (VersaLogic, Eugene, OR).

Online Supplemental Material

Time-lapse videos that accompany Figures 2, 3, and 5 are available online. These include Movies 1 and 2: GFP-M6; Movies 3 and 4: GFP-M6tail; Movies 5 and 6: GFP-M6(K157R). Three figures and associated text characterizing the properties of GFP-M6(K157R)–associated vesicles are also available. These

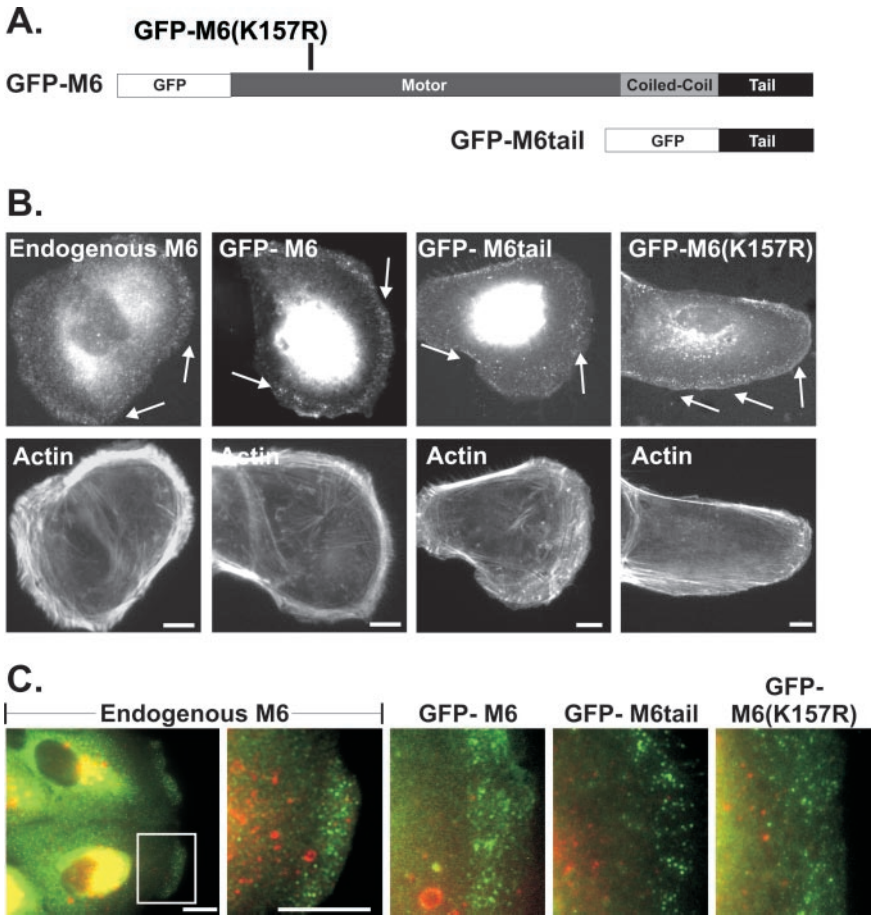

Figure 1. Myo6 and GFP-tagged myo6 constructs localize to peripheral uncoated vesicles. (A) Schematic of GFP-myo6 constructs. The motor domain point mutation, K157R, is indicated. (B) Staining of ARPE-19 cells using rabbit anti-myo6 antibodies (endogenous M6) or cells transfected with the GFP fusion constructs, counterstained for F-actin with rhodamine-conjugated phalloidin. Arrows point out myo6-associated peripheral vesicles. (C) Double-labeled images visualizing endogenous myo6 or GFP-myo6 fusion constructs (green) and the early endosome marker EEA1 (red). Scale bars, 10 μm.

include Supplementary Figure 1: GFP-M6(K157R), like wild-type myo6, targets to uncoated vesicles. Supplementary Figure 2: Overexpression of the myo6 motor domain mutant, GFP-M6(K157R), blocks trafficking of transferrin to the early endosome. Supplementary Figure 3. Overexpression GFP-M6(K157R) blocks trafficking of transferrin at the uncoated vesicle stage.

RESULTS

In cultured ARPE-19 epithelial cells, myo6 is found associated with uncoated endocytic vesicles located in peripheral actin-rich regions (Aschenbrenner *et al.*, 2003). These vesicles lack both clathrin and the early endosome marker, EEA1 (Figure 1, B and C; Aschenbrenner *et al.*, 2003). GFP-tagged myo6 (GFP-M6; Figure 1A) targets to these uncoated vesicles (Figure 1, B and C), which were monitored by time-lapse fluorescence digital microscopy at 25°C (Figure 2; Supplementary Movies 1 and 2).

GFP-M6–decorated vesicles exhibited complex trajectories within cell peripheries, with combinations of long unidirectional movements either laterally or toward more central regions interspersed with pauses (Figure 2, A and B). Vesicle velocity was variable over time (Figure 2C). Statistical analysis of >250 vesicles revealed that the distribution of instantaneous velocities was broad, averaging 38.4 ± 16.6 nm/s (Figure 3A). Although the GFP-M6–associated vesicles appeared to take a very circuitous route through cell peripheries (Figures 2, Ad and B), vector analysis, which compared the start and end points of vesicle tracks, revealed that all vesicles tracked exhibited a net vector inward into the cell (Figure 2D). The average net distance traveled was 1.8 ± 1.4 μm (Figure 3B), with distances ranging between 0.3 and 5.5 μm. This variation was expected, as the distance required for transport would differ depending on the vesicle's initial position and the position of the presumed destination early endosome. Overall, the distance traveled was consistent with the width of the actin mesh seen in ARPE-19 cells (Figure 1B) and suggests that myo6 was recruited to move vesicles out of actin-rich regions and not further into the cell.

Pulse-chase experiments following transferrin trafficking had revealed a 2–10-min delay between formation of a new clathrin-coated vesicle and delivery of the vesicle contents to the endosome (Hopkins, 1983; Hanover *et al.*, 1984; Eskelinen *et al.*, 1991; Trischler *et al.*, 1999). Although the actual time varied between cell lines, these results suggested that uncoated vesicles in all cell types had a relatively short lifetime of a few minutes. We calculated the lifetime of >250 GFP-M6–decorated vesicles by comparing the timing of their first appearance within the cell (when GFP-M6 was recruited upon vesicle uncoating) to their disappearance (when GFP-M6 departs, an event we correlate with fusion with the early endosome as myo6 is not present on this destination compartment). Taking into account vesicles with short lifetimes (<40 s) and the fact that the final movement of each uncoated vesicle, which culminated in fusion with the early endosome, was missed in our analysis, we calculated an average lifetime of 4.5 ± 2.7 min (Figure 3C). This lifetime is consistent with their identity as uncoated vesicles.

Our analysis of individual myo6-associated uncoated vesicles illuminated several types of membrane dynamics not previously described for this compartment. The most

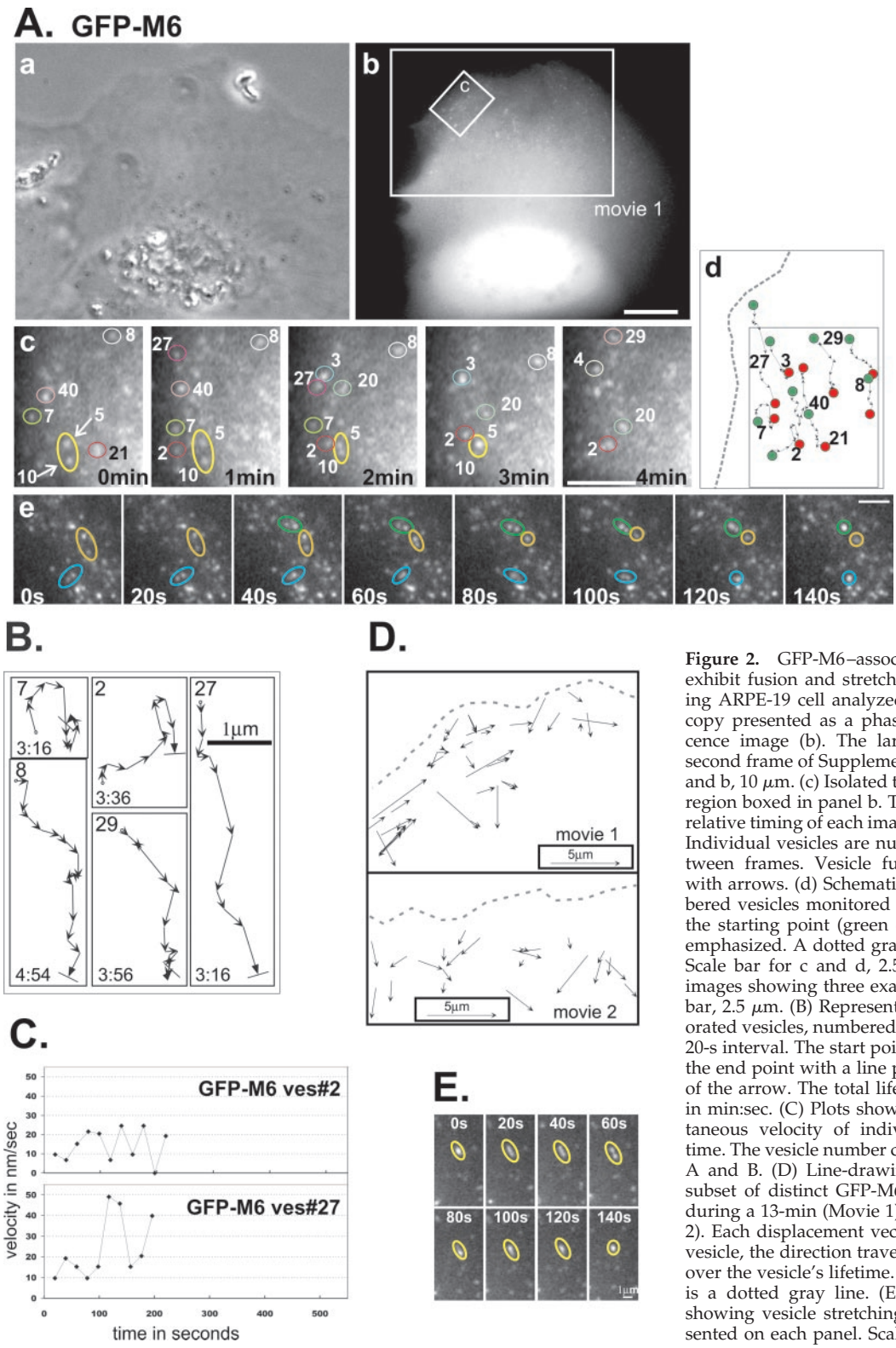

Figure 2. GFP-M6–associated vesicles are motile and exhibit fusion and stretching. (A) A GFP-M6–expressing ARPE-19 cell analyzed by time-lapse videomicroscopy presented as a phase contrast (a) and a fluorescence image (b). The larger box corresponds to the second frame of Supplementary Movie 1. Scale bar for a and b, 10 μm. (c) Isolated time-lapse images of the small region boxed in panel b. The cell edge is at the left. The relative timing of each image is presented on each panel. Individual vesicles are numbered to allow tracking between frames. Vesicle fusion events are demarcated with arrows. (d) Schematic showing the tracks of numbered vesicles monitored in panel c (boxed area), with the starting point (green dot) and end point (red dot) emphasized. A dotted gray line depicts the cell border. Scale bar for c and d, 2.5 μm. (e) Isolated time-lapse images showing three examples of vesicle fusion. Scale bar, 2.5 μm. (B) Representative tracks of GFP-M6–decorated vesicles, numbered in A, panel c. Each arrow is a 20-s interval. The start point is demarcated with an "o," the end point with a line perpendicular to the direction of the arrow. The total lifetime of the vesicle tracked is in min:sec. (C) Plots showing the change in the instantaneous velocity of individual vesicles tracked over time. The vesicle number corresponds to those shown in A and B. (D) Line-drawing showing a representative subset of distinct GFP-M6–associated vesicles evident during a 13-min (Movie 1) or a 16-min window (Movie 2). Each displacement vector shows the position of the vesicle, the direction traveled, and the distance covered over the vesicle's lifetime. The outline of the cell border is a dotted gray line. (E) Isolated time-lapse images showing vesicle stretching. The relative timing is presented on each panel. Scale bar, 1 μm.

commonly visualized event was fusion between GFP-M6–associated vesicles. Fusion was characterized by the apparent meeting of two vesicles, producing a single vesicle with approximately twice the apparent fluorescent intensity that remained as a single entity for the remainder of the vesicle's lifetime (Figure 2A; Movies 1 and 2). In a 250-μm^2 area an average of 1.4 $\pm$ 1.3 fusion events were observed per min, with the number of vesicle fusions ranging from 0 to 4 events per min. Overall, approximately 1 in 10 vesicles participated in a fusion event, suggesting that myo6-based transport serves two purposes: not only does it allow transport through actin-rich

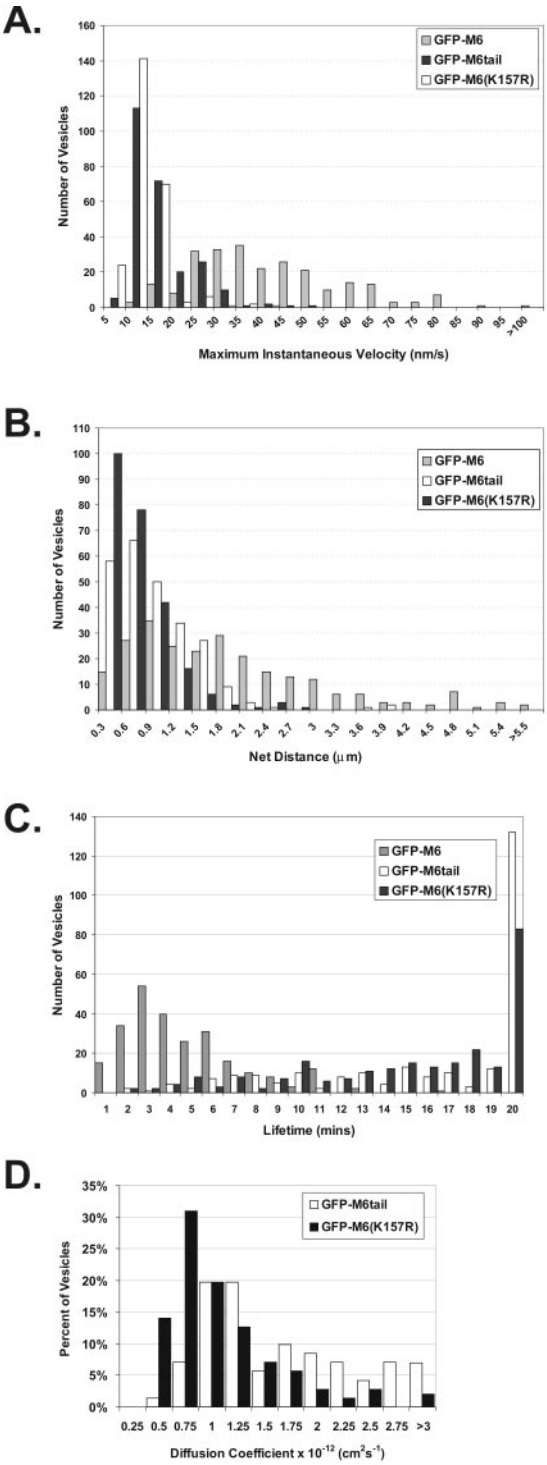

Figure 3. Uncoated vesicles exhibit significant movement and a short lifetime only when associated with functional myo6. Two hundred fifty vesicles were tracked in cells expressing either GFP-M6 (gray bars), GFP-M6tail (black bars), or GFP-M6(K157R) (white bars). (A) Histogram showing the maximum instantaneous velocity in nm/s for each vesicle tracked. (B) Histogram showing net distance in micrometers traveled by each vesicle. (C) Histogram of the total lifetime in minutes exhibited by each vesicle. (D) Histogram of the diffusion coefficients obtained from tracking vesicles.

regions, but it also uses its association with the actin cytoskeleton to enable vesicle fusion.

Vesicle separation or fission events were not seen; however, we noted multiple occurrences of vesicle stretching, characterized by pulling of a vesicle to produce an elongated shape, followed by what appeared to be separation into two less-fluorescent daughter vesicles (Figure 2E). In all cases these fission events were unsuccessful, and the stretched vesicle returned to its original shape (Figure 2E). An average of 0.75 ± 0.5 stretching events were seen per min within a 250-μm^2 area.

Uncoated Vesicle Movement Requires myo6 Motor Activity

In all cells analyzed by time lapse, GFP-M6–decorated vesicles appeared, exhibited movements and then disappeared (see Supplementary Movies 1 and 2). We hypothesized that the observed movements were due to myo6 motor activity. To test this we used a construct that fused GFP to the globular cargo-binding tail of myo6 but lacked a motor domain (GFP-M6tail; Figure 1A). When expressed in ARPE-19 epithelial cells, GFP-M6tail targeted to peripherally located vesicles (Figure 1, B and C). Time-lapse microscopy revealed that the GFP-M6tail–associated vesicles exhibited short, slow movements interspersed with pauses (Figure 4A–C; Supplementary Movies 3 and 4). The lack of directionality suggested that the vesicles were exhibiting Brownian-like motion. Quantitation of 250 vesicles revealed an average maximal instantaneous velocity of 13.3 ± 6.9 nm/s (Figure 3A) with an average of 0.7 ± 0.5 μm traveled (Figure 3B), both significantly depressed from that seen for GFP-M6–expressing cells ($p < 0.001$). Therefore, myo6 motor activity is important for uncoated vesicle movement.

The vesicle stretching events noted in GFP-M6–expressing cells, were not detected in GFP-M6tail–expressing cells, confirming that myo6 motors and not other motor proteins, are generating force during these events. When vesicle fusion was evaluated in GFP-M6tail–expressing cells, however, it was evident that, although trapped in cell peripheries, the uncoated vesicles did still exhibit fusion (Figure 4A). To quantify these events, we monitored ~120 vesicles over a 13.3-min period and 16.6% of the GFP-M6tail–associated vesicles exhibited vesicle fusion; however, this high percentage is misleading because of the long vesicle lifetime (see below). The overall fusion rate was 0.37 fusion events per min per 250 μm^2, a level significantly lower than that seen in GFP-M6–expressing cells, suggesting that myo6 motor activity modulates or accelerates the fusion rate.

Disruption of myo6 Motor Function Increases the Uncoated Vesicle Lifetime

Previous studies had shown that overexpression of GFP-M6tail led to a 15-min delay in transferrin trafficking to the early endosome (Aschenbrenner *et al.*, 2003). Consistent with this delay, GFP-M6tail–associated vesicles monitored by time-lapse microscopy exhibited a dramatic increase in vesicle lifetime, averaging 15.4 ± 5.6 min (Figure 3C). No difference in lifetime was noted based on vesicle position within the cell (unpublished data). This lifetime is likely an underestimate because cells were recorded for 20–22 min, and of 250 vesicles monitored the majority (65–85%) were still present at the movie's end. Therefore only a small percentage of vesicles disappeared as a result of early endosome fusion, suggesting that the defect in trafficking to the early endosome increases the apparent vesicle lifetime.

Vector analysis monitoring the start and end position of each vesicle confirmed that the GFP-M6tail–associated ves-

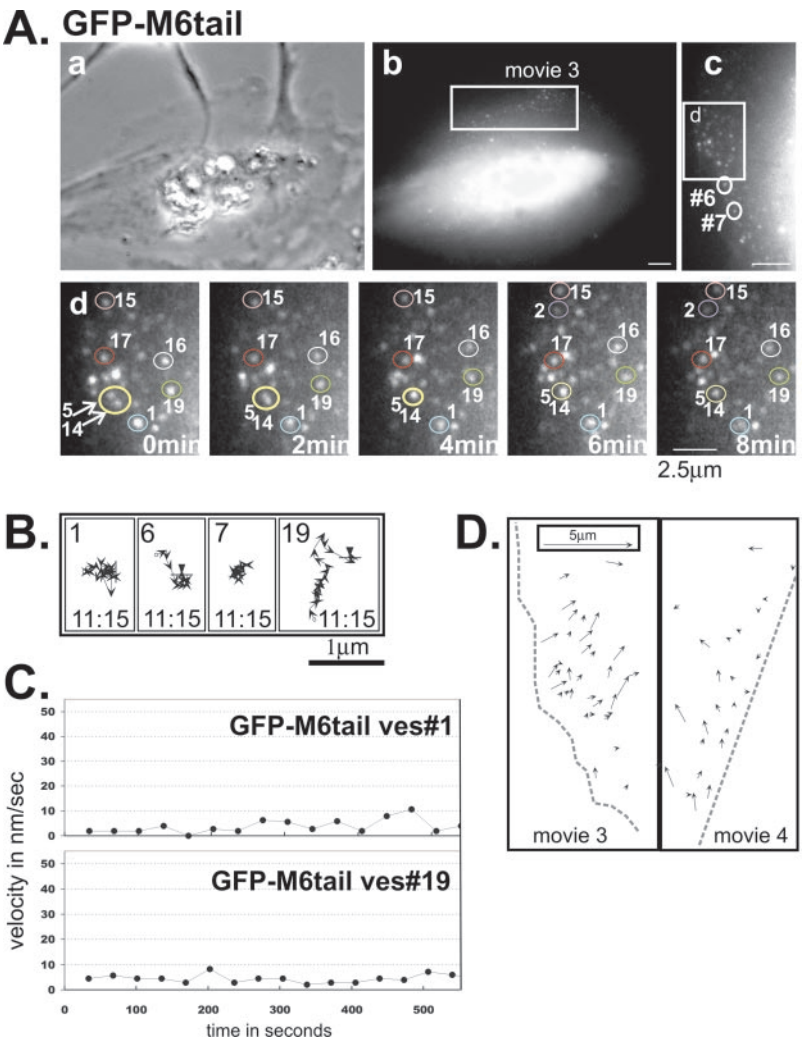

Figure 4. Analysis of GFP-M6tail–associated vesicles reveals a requirement for the myo6 motor domain for vesicle movement. (A) Images of a GFP-M6tail–expressing ARPE-19 cell monitored by time lapse, presented as a phase contrast (a) and a fluorescence image (b). The boxed region corresponds to Supplementary Movie 3 and is enlarged and rotated counterclockwise in panel (c). (d) Isolated images from the time-lapse movie of the cell portion boxed in panel (c). The cell edge is at the left of the panel and the relative timing of each image is indicated. Representative individual vesicles are numbered in panels (c) and (d). Vesicle fusion events evident in panel (d) are demarcated with arrows. Scale bar for a and b, 10 μm; c, 5 μm; d, 2.5 μm. (B) Representative tracks of GFP-M6tail–decorated vesicles. The numbers correspond to the vesicles circled in A, panels (c) and (d), and tracks are as described for Figure 2. (C) Plots showing the change in the instantaneous velocity of individual vesicles tracked over time. (D) Line drawing depicting the direction and distance traveled for a series of distinct GFP-M6tail–associated vesicles present simultaneously over a 20-min period in two cells (Supplementary Movies 3 and 4; see legend for Figure 2D).

icles were not moving great distances (Figure 4D). However, analysis of many cells revealed that over the long vesicle lifetime there was a trend of net movement inward for many vesicles tracked. Inspection of phase-contrast images suggested that this was not due to general cell contraction. GFP-M6tail expression in epithelial cells causes a delay, not a block, in transferrin trafficking; given 30 min, the contents of the uncoated vesicles can be delivered to the early endosome (Aschenbrenner *et al.*, 2003). We therefore hypothesized that the inward movement of GFP-M6tail–associated uncoated vesicles could reflect an alternate mechanism for slow vesicle trafficking in the absence of myo6.

Uncoated Vesicle Movement Is Not Linked to Retrograde Actin Flow

One explanation for the apparent slow inward movement of GFP-M6tail–associated vesicles could be the action of residual endogenous myo6 associated with these vesicles. However, previous studies have shown that this construct effectively displaces endogenous myo6 off of the surface uncoated vesicles, even when expressed at low levels (Aschenbrenner *et al.*, 2003). As all GFP-M6tail–expressing cells analyzed, regardless of expression level, exhibited this slow inward flow, this simple explanation seemed insufficient to explain this trend.

The GFP-M6tail–associated vesicles exhibited Brownian-like motion, with periods of nonmovement interspersed with short randomly oriented ~10-nm/s movements (Figure 4, B and C), suggesting some freedom of motion. Therefore, the net vesicle movement could be due to diffusion coupled to endosome capture. We theorized that any vesicle that exited the actin meshwork would immediately fuse with an early endosome because these endosomes are abundant outside the actin mesh. Therefore, this fusion event could serve as a mechanism to bias diffusion thereby producing a net inward vesicle flow.

Alternatively, because the cell region that accumulated uncoated vesicles in GFP-M6tail–expressing cells was highly actin-rich, we hypothesized that the slow net vesicle influx could be due to vesicle coupling to retrograde actin flow. Retrograde actin flow describes the process whereby actin polymerization at the plasma membrane is coupled to myosin II–dependent force production, resulting in a net inward flow of actin and associated components (reviewed in Cramer, 1997). Retrograde actin flow is not commonly observed in nonmotile epithelial cells, but retrograde flow in motile fibroblasts and nerves can generate inward transport of actin-associated components at a rate of 1–7 μm/min (16–116 nm/s; Cramer, 1997). This rate is similar to the maximal velocity of GFP-M6tail–associated vesicles, making

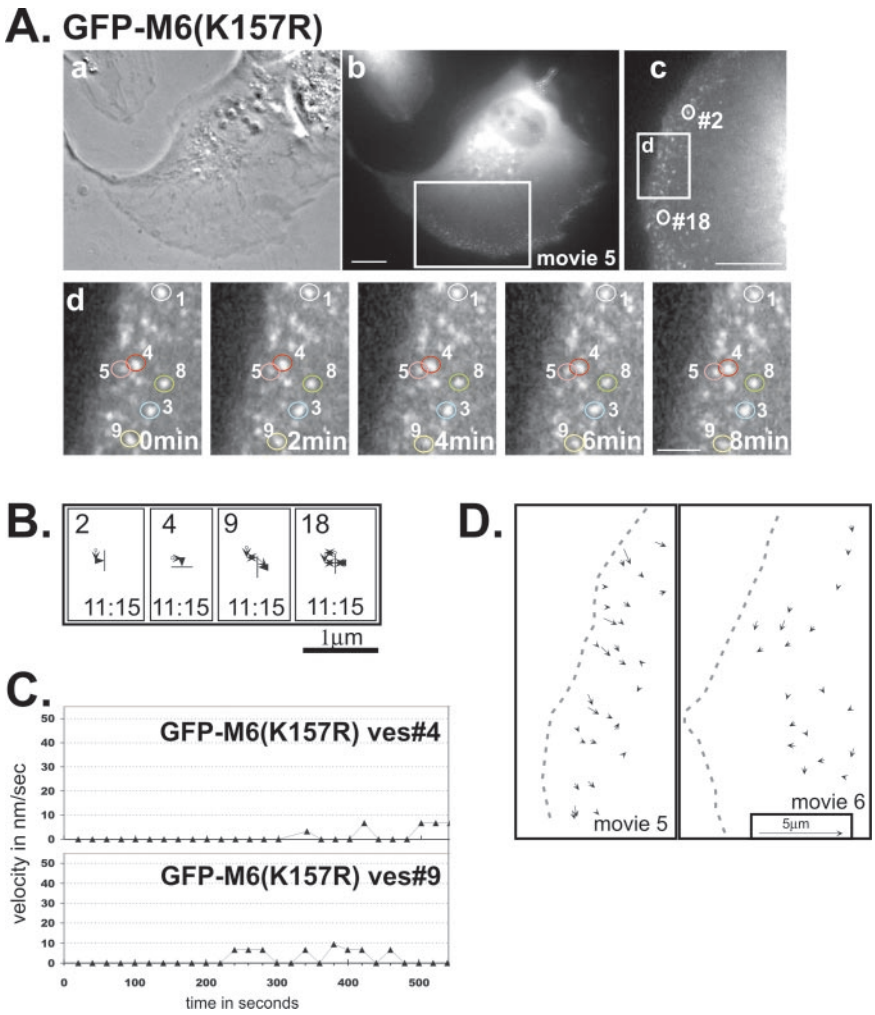

Figure 5. Analysis of GFP-M6(K157R)–associated vesicles reveals no movement, suggesting this mutation causes tight binding to the actin cytoskeleton. (A) Phase contrast (a) and fluorescence images (b) of a GFP-M6(K157R)–expressing ARPE-19 cell monitored by time-lapse video. Boxed region corresponds to Supplementary Movie 5 and is enlarged and rotated clockwise in panel (c). (d) Isolated images from the time-lapse movie of the cell portion boxed in panel (c). The cell edge is at the left of the panel and the relative timing of each image is presented on each panel. Individual vesicles are numbered. The scale bars are as in Figure 4. (B) Representative tracks showing the movements of GFP-M6(K157R)–decorated vesicles. The numbers correspond to the vesicles circled in A, panels (c) and (d), and tracks are as described for Figure 2. (C) Plots showing the change in the instantaneous velocity of individual vesicles tracked over time. (D) Line-drawing depicting the direction and distance traveled for a series of distinct GFP-M6(K157R)–associated vesicles present simultaneously during a 20-min period in two cells (Supplementary Movies 5 and 6; see legend for Figure 2D).

retrograde flow a reasonable explanation for the apparent inward movement.

To distinguish between these two theories, retrograde flow vs. vesicle diffusion and capture, we created a myo6 mutant predicted to bind irreversibly to F-actin. GFP-M6(K157R), contains a point mutation in the ATP-binding site (Figure 1A). The K157R mutation is homologous to the P-loop K185R mutation shown in the *Dictyostelium* myosin II system to fail to complement myosin II null mutations (Ruppel and Spudich, 1996). In myosin II, the K185R mutation caused a defect in myosin ATP binding. Furthermore, the mutated myosin exhibited no ATPase activity and was defective in actin filament sliding due to rigor-like actin binding (Ruppel and Spudich, 1996). We predicted that by introducing the K157R mutation into myo6, cells expressing this mutated version would exhibit actin-bound uncoated endocytic vesicles, allowing us to evaluate the importance of retrograde flow and free diffusion on vesicle trafficking.

When expressed in ARPE-19 cells, GFP-M6(K157R) targeted to peripherally located vesicles distinct from early endosomes, a subset of which contained the transferrin receptor (Figure 1, B and C; Supplemental Figure 1A). These vesicles were uncoated, as they did not contain clathrin (percent overlap 4.4 ± 0.4%; Supplemental Figure 1B). This localization to uncoated vesicles was expected, as the tail domain, and not the motor domain, is required for targeting (Aschenbrenner *et al.*, 2003).

Time-lapse video microscopy revealed that GFP-M6(K157R)–associated uncoated vesicles displayed essentially no movement (Figure 5, A–C; Supplementary Movies 5 and 6). These vesicles also exhibited no fusion events (200 vesicles monitored), nor was vesicle stretching seen in GFP-M6(K157R)–expressing cells (Movies 5 and 6). Analysis of 250 vesicles revealed few instances of directional movement as judged by velocity measurements (average maximal velocity = 10.6 ± 10.9 nm/s; Figure 3A) and the average distance traveled was 0.5 ± 0.4 μm. (Figure 3B). Both measurements are statistically lower than that seen for GFP-M6tail–associated vesicles ($p < 0.001$), suggesting that the K157R mutation produced vesicles with rigor-like strong attachment to the peripheral actin.

To directly evaluate the effects of GFP-M6(K157R) expression on vesicle diffusion, we computed the mean squared displacement (MSD) for GFP-M6tail– and GFP-M6(K157R)–associated vesicles and plotted them as a function of time to determine the apparent two-dimensional diffusion coefficients associated with these vesicle populations (200 vesicles analyzed). In both cases, the majority of the vesicles exhibited plots with a downward curved parabolic curve, indicating confined motion. Seventy-one vesicles for both constructs exhibited a more linear correspondence between MSD and time, allowing us to calculate their apparent diffusion coefficients (Figure 3D). GFP-M6tail–associated vesicles had a diffusion coefficient of 1.42 ± 1.24 × 10^{-12} cm^2

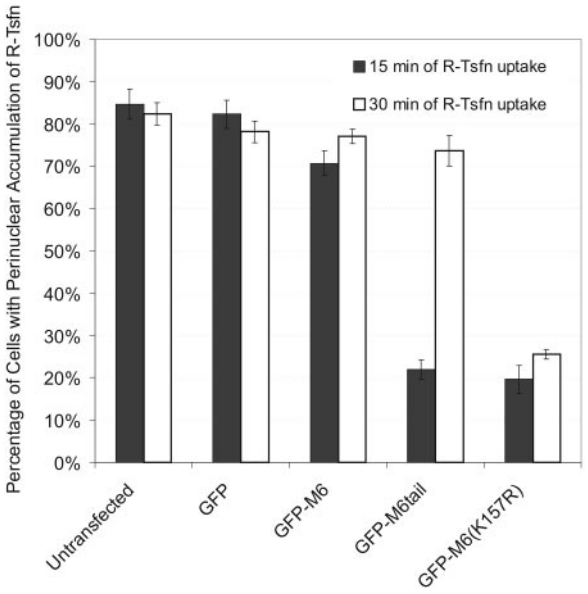

Figure 6. Expression GFP-M6(K157R) blocks transferrin trafficking and it cannot be rescued by extending uptake time. GFP-, GFP-M6–, GFP-M6tail–, and GFP-M6(K157R)–transfected cultures were incubated with rhodamine-conjugated transferrin (R-Tsfn). The histogram shows the percentage of transfected and untransfected cells exhibiting labeling of the pericentriolar endosomes with the endocytosed R-Tsfn after 15 min (black bars) or 30 min (white bars). See Supplementary Figure 2 for primary data. More than 300 cells were counted per time point and the data are representative of three experiments.

s^{-1}, a value similar to the three-dimensional diffusion coefficient described for chromaffin granules docked on the actin cytoskeleton (Oheim and Stuhmer, 2000). GFP-M6(K157R)–associated vesicles exhibited a significantly depressed diffusion coefficient ($p < 0.001$) of $0.76 \pm 0.65 \times 10^{-12}$ cm^2 s^{-1}. Therefore, GFP-M6(K157R)-associated vesicles exhibited an apparent decrease in two-dimensional diffusion.

We predicted that if retrograde flow was a mechanism for vesicle influx, then the actin bound GFP-M6(K157R)–associated vesicles should exhibit an inward flow similar to that seen for GFP-M6tail–expressing cells. Remarkably, vector analysis of the GFP-M6(K157R)–associated vesicles over their lifetime revealed no net inward vesicle flow (Figure 5D). Therefore retrograde actin flow does not serve as a mechanism for vesicle influx, supporting the model that diffusion followed by endosome capture is responsible for the vesicle movements seen in GFP-M6tail–expressing cells.

GFP-M6(K157R)–associated vesicles exhibited long lifetimes in our time-lapse analysis (average lifetime = 16.4 ± 5.6 min; Figure 3C). Essentially all vesicles were still present at the movie's end (85–92%; see Supplementary Movies 5 and 6, movie lengths 20–22 min), making 16 min an underestimate. Therefore tight association with the peripheral actin also lengthened vesicle lifetime, suggesting a block in trafficking.

An Actin-bound myo6 Motor Mutant Blocks Transferrin Trafficking to the Early Endosome at the Uncoated Vesicle Stage

The block in transferrin trafficking seen in GFP-M6tail–expressing cells can be overcome by extending the incubation time to 30 min (Figure 6; Supplementary Figure 2; Aschenbrenner *et al.*, 2003). We theorized that, if rescue was due to diffusion of GFP-M6tail–associated vesicles followed by their early endosome capture, then GFP-M6(K157R)–expressing cells, with their actin-bound vesicles, would not be sensitive to this type of rescue.

ARPE-19 cells were transfected with the GFP constructs shown in Figure 1A, incubated with rhodamine-conjugated transferrin (R-Tsfn) for 15 or 30 min and then scored for transferrin accumulation in the pericentriolar early endosome compartment. Seventy to 80% of control transfected and untransfected cells exhibited a prominent pericentriolar accumulation of R-Tsfn after 15-min uptake (Figure 6, Supplementary Figure 2; Aschenbrenner *et al.*, 2003). In contrast, GFP-M6(K157R) overexpression caused a drastic decrease in steady state R-Tsfn uptake at 15 min, with only 19.6 ± 3.3% of cells exhibiting a pericentriolar accumulation (Figure 6; Supplementary Figure 2). These results are similar to those reported for cells expressing GFP-M6tail (22.0 ± 2.3%), confirming that GFP-M6(K157R) expression disrupts transferrin trafficking. Pulse-chase experiments comparing the location of the endocytosed R-Tsfn to GFP-M6(K157R) confirmed that the block in trafficking was at the uncoated vesicle stage (Supplementary Figure 3 and associated text). As predicted, the block in trafficking was not rescued by extending the time period; 25.6 ± 1.2% of GFP-M6(K157R)–transfected cells exhibited a pericentriolar accumulation of R-Tsfn after 30-min uptake (Figure 6; Supplementary Figure 2). This lends further support to the diffusion and capture model for vesicle trafficking out of the actin mesh in the absence of myo6 motor activity.

Actin Is a Barrier to Uncoated Vesicle Trafficking

Our analysis of myo6 mutants suggested that actin was a barrier slowing uncoated vesicle trafficking to the early endosome. If this were the case, we predicted that actin depolymerization should accelerate the rate of transferrin delivery to the early endosome. We used the F-actin–depolymerizing drug latrunculin A (LatA) (Spector *et al.*, 1983), which sequester G-actin monomers. Titration experiments revealed that nanomolar LatA concentrations were sufficient to remove the peripheral actin meshwork from ARPE-19 epithelial cells without significantly altering cell attachment or cell shape (Figure 7A). Treatment with 0.015 μM LatA had no effect on the transferrin endocytosis rate in ARPE-19 cells, as judged by an ELISA-based assay that quantified biotinylated transferrin uptake (Figure 7B). In addition, pulse-chase experiments following R-Tsfn and comparing its location to clathrin confirmed that treatment with LatA had no effect on the rate of transferrin exit from clathrin-coated pits and vesicles (Figure 7C). Therefore, depolymerizing the peripheral actin cytoskeleton had no effect clathrin-coated vesicle formation or uncoating, allowing us to directly test the effects of LatA on the next step, the delivery of components to the early endosome.

To determine early endosome delivery kinetics, we allowed cells treated with DMSO or LatA to endocytose R-Tsfn for fixed time periods ranging from 1 to 15 min at 37°C and then quantified the percent of cells where R-Tsfn had reached the pericentriolar early endosome (see MATERIALS AND METHODS). In DMSO-treated cells, R-Tsfn maximally reached the early endosome after 5–7 min (Figure 7D). In LatA-treated cells, R-Tsfn delivery to the early endosome was accelerated, reaching the pericentriolar region within 2–3 min ($p < 0.001$). A similar acceleration was observed in LatA-treated cells when the location of endocytosed transferrin was compared with the early endosome marker, EEA1 (unpublished data). This acceleration suggests that actin is a

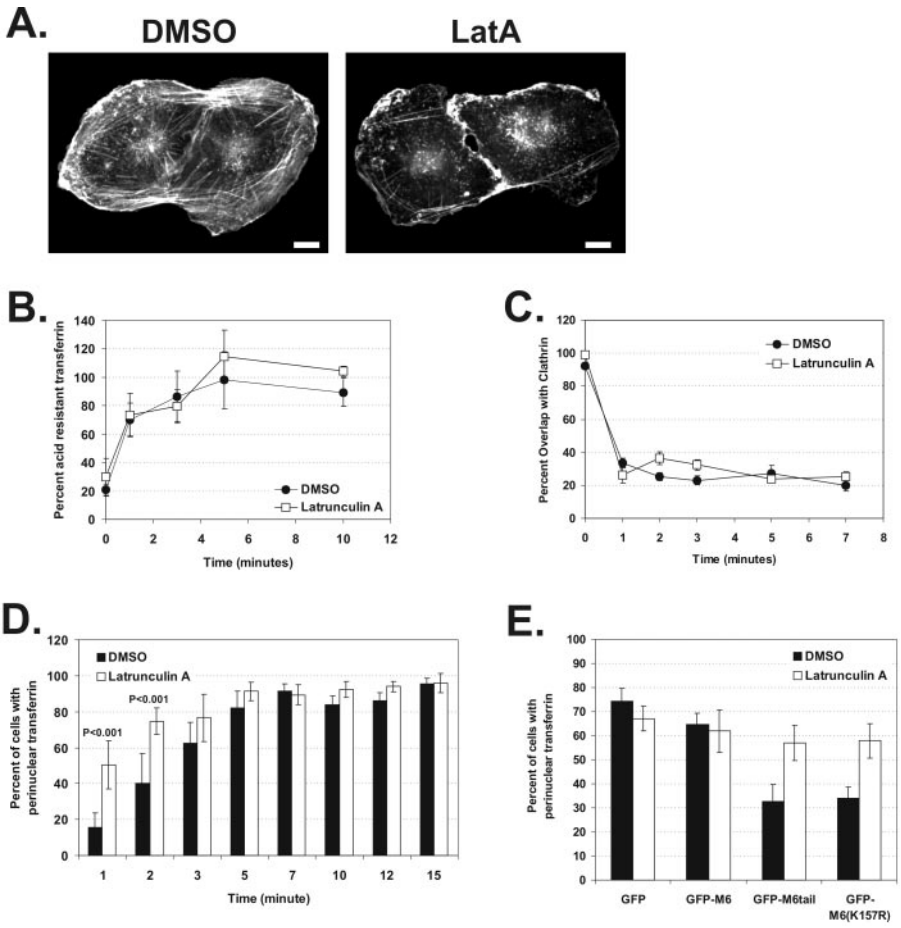

Figure 7. Removal of the actin barrier in ARPE-19 cells accelerates trafficking to the early endosome and rescues the trafficking defects seen upon GFP-M6tail and GFP-M6(K157R) expression. (A) Fluorescence staining of F-actin in cells treated for 30 min with DMSO or 0.015 μM latrunculin A. Scale bars, 10 μm. (B and C) Kinetics of transferrin endocytosis and transferrin exit from clathrin-coated vesicles as judged by pulse-chase experiments in cells incubated in the presence of DMSO (●) or latrunculin A (□). (B) Quantification of the endocytosis of biotinylated transferrin. Shown is a representative example of four experiments. (C) Quantitation of the exit of transferrin from clathrin-coated vesicles, as assayed by the percent overlap between clathrin and endocytosed R-Tsfn during the course of a pulse-chase experiment. (D and E) Delivery of transferrin to the pericentriolar early endosome, as judged by steady state uptake experiments in the presence of DMSO (black bars) or latrunculin A (white bars). (D) Histogram showing the percent of cells exhibiting delivery of R-Tsfn to the pericentriolar early endosome at fixed uptake times. More than 600 cells were counted per time point. (E) Histogram showing the percent of transfected cells exhibiting delivery of endocytosed R-Tsfn to the pericentriolar early endosome after 15 min of uptake. More than 500 cells were counted per construct.

barrier to uncoated vesicle trafficking to the early endosome and that actin's presence causes a 3–5-min delay in endosome delivery equivalent to the normal uncoated vesicle lifetime.

Transferrin-containing vesicles accumulate in peripheral actin-rich regions of GFP-M6tail– and GFP-M6(K157R)–expressing cells, thereby blocking delivery to the early endosome. We hypothesized that F-actin depolymerization should rescue this phenotype. We first evaluated the effects of actin depolymerization on cells transfected with GFP and GFP-M6. These control experiments revealed that the presence of DMSO coupled with the exposure to transfection reagent resulted in a slower net rate of steady state transferrin uptake compared with untransfected controls. After 15 min of uptake in the presence of DMSO or LatA, 60–75% of GFP- or GFP-M6–transfected cells exhibited a pericentriolar R-Tsfn accumulation, a number significantly less than the ~95% seen for untransfected cells after 15 min (Figure 7D). Although trafficking was slower, in the presence of DMSO, cells transfected with GFP-M6tail and GFP-M6(K157R) still exhibited a significant block in transferrin trafficking, with only 32.7 ± 7.1 and 34.1 ± 4.5% of cells exhibiting a pericentriolar accumulation, respectively. After treatment with LatA, however, 57.0 ± 7.3% of GFP-M6tail–transfected cells and 57.9 ± 7.3% of GFP-M6(K157R)–transfected cells exhibited pericentriolar transferrin accumulation, levels equivalent to those seen in controls. Therefore the block in trafficking seen upon GFP-M6tail and GFP-M6(K157R) overexpression is due to trapping in the actin cytoskeleton, and this block can be released by removing the F-actin barrier.

DISCUSSION

Previous studies using pulse-chase methods in cultured cell lines had suggested that there was a short-lived uncoated vesicle population found near the plasma membrane that ultimately fused with the early endosome (Hopkins, 1983; Hanover *et al.*, 1984; Eskelinen *et al.*, 1991; Trischler *et al.*, 1999). In this study we present the first characterization of these nascent uncoated endocytic vesicles, showing that they are motile, exhibiting net movement into the cell. A myosin, myo6, is responsible for their movement. In the absence of a myo6 motor, only slow diffusion-based vesicle movement to the early endosome is evident, a movement that was not due to retrograde actin flow. Actin instead is a physical barrier to uncoated vesicle trafficking. Accelerated vesicle movement out of the actin mesh is due to myo6 motor activity and results in a short vesicle lifetime. Therefore the molecular motor myo6 is specifically recruited to extricate nascent vesicles from the actin mesh to allow for timely early endosome fusion.

An important question is whether GFP-tagged myo6 is a good tracer for uncoated vesicle trafficking. A number of proteins are transiently found as uncoated vesicle components. For example, both the small GTPase Rab5 and the transferrin receptor, can be detected on uncoated vesicles, but in both cases this reflects only a small fraction of the total

cell population. The majority of Rab5 is either cytoplasmic, in a guanine-nucleotide dissociation inhibitor (GDI)-complexed form (Pfeffer *et al.*, 1995) or is associated with early endosomes (Gorvel *et al.*, 1991); reviewed in Zerial and McBride, 2001), whereas the transferrin receptor is evident in the membrane of all endocytic and exocytic compartments with an enrichment in the recycling endosome (Hopkins, 1983; Hanover *et al.*, 1984; Eskelinen *et al.*, 1991; Trischler *et al.*, 1999; reviewed in Mukherjee *et al.*, 1997). A similar heterogeneous distribution exists for GIPC, an adapter protein, which is also evident on coated vesicles, the Golgi, and on other small vesicles found throughout the cell cytoplasm (De Vries *et al.*, 1998; Liu *et al.*, 2001; Aschenbrenner *et al.*, 2003). Myo6 is the only protein identified to date that specifically marks the position of uncoated vesicles and does not remain with it after delivery to the early endosome. The GFP-M6 construct used in this study exhibits a location essentially identical to the endogenous myo6, specifically targeting to endocytic vesicles that uncoat in actin-rich cell peripheries (Aschenbrenner *et al.*, 2003). Therefore, GFP-M6 is a good tracer for trafficking of this specific type of nascent endocytic vesicles.

After recruitment of myo6, uncoated vesicles exhibited net movement toward the cell interior. The motile properties of myo6 have been characterized using baculovirus-expressed fragments containing either a single head (motor) domain or a heavy meromyosin-like fragment containing two heads bridged by the coiled-coil domain. The observed velocities at 25°C in the in vitro actin-filament sliding assays ranged from 60 nm/s for a singled-headed construct (Wells *et al.*, 1999) to 300 nm/s for the double-headed constructs (Homma *et al.*, 2001; Rock *et al.*, 2001; Yoshimura *et al.*, 2001).

Myo6 is a processive motor, but the average processive run length was only 226 nm, suggesting a maximum of 1 s of movement before pausing or falling off the actin filament (Rock *et al.*, 2001). The velocity of the GFP-M6–decorated uncoated vesicles at 25°C was much lower than the in vitro rates for myo6, at 38.4 nm/s, although velocities of up to 80 nm/s were detected. These "instantaneous" velocity calculations actually reflected an average velocity over the 20-s interval between video frames, a much less-frequent sampling than that used for sliding filament assays. If myo6 exhibited one processive run of 226 nm during the 20-s interval, a net velocity of 11.3 nm/s would have been evident in our system, a velocity that was easily detectible. Because our velocities were at least three times this rate, GFP-M6 made on average 3–5 productive runs during each 20-s interval. Based on our observations of vesicle stretching, there are multiple myo6 motors on each vesicle exerting opposing forces, a process that would also decrease net velocity. Ultimately, as expression of myo6 mutants produced vesicles with no movement, we conclude that the movements we did see for GFP-M6–associated vesicles was due to the intrinsic motor activity of myo6 and that no other actin-based motor was associated with these vesicles. This is the first example of myo6-based movement in vivo.

The GFP-M6–decorated uncoated vesicles commonly exhibited homotypic fusion events. These events were not seen in GFP-M6(K157R)–expressing cells, suggesting that freedom of movement was important for fusion to occur and that anchoring to the actin cytoskeleton was not sufficient. All the vesicle fusion events appeared to occur before early endosome fusion, based on both the vesicle position and the presence of myo6. This fusion could be evidence of receptor sorting events before endosome delivery.

On exit from the actin-rich peripheries, GFP-M6–associated vesicles disappeared from view. The signal that triggers myo6 departure after endosome fusion remains to be identified; however, motor activity is important for myo6 release. A peripheral subpopulation of small EEA1-positive endosomes can contain myo6, and these endosomes were extensively labeled with the GFP-M6tail construct (Aschenbrenner *et al.*, 2003). The presence of this endosome population supports a model whereby myo6 is present during fusion but is released after fusion is complete, perhaps through the pulling action of its motor domain. Our study does not rule out an additional role in regulating endosomal fusion. After myo6 departure, the movement of early endosomes further along the endocytic pathway is mediated by microtubule motors under Rab5 regulation (Goodson *et al.*, 1997; Nielsen *et al.*, 1999).

Uncoated vesicles are universally present in all cells as an intermediate in endocytic trafficking between clathrin-coated vesicles and the early endosome. In some cell types, such as polarized epithelial cells with a terminal web domain, actin would serve as a barrier to uncoated vesicle delivery. Therefore we would propose that epithelia present in *Snell's waltzer* mice, which lack myo6, must utilize vesicle diffusion followed by endosome capture as the major mechanism for delivery to the early endosome. In other cell types, such as fibroblasts, which lack dense actin-rich regions, there would not be a barrier, and endosome delivery could occur unimpeded. Indeed, we have found that expression of myo6 mutants has no effect on trafficking in fibroblasts, confirming that myo6 is specifically involved in trafficking through actin-rich regions only (our unpublished results).

In secretory cell types, the actin cortical network is a barrier to exocytosis at the plasma membrane (reviewed in Eitzen, 2003). In these systems, actin serves a scaffolding role and is required to anchor secretory vesicles as a readily releasable pool (Sankaranarayanan *et al.*, 2003). In some cases, this anchoring requires a myosin (Rose *et al.*, 2002; Rudolf *et al.*, 2002), whereas in other cases, such as GLUT4 delivery to the adipocyte plasma membrane, a plus-end–directed unconventional myosin, myo1C, may play a role in vesicle delivery across the barrier toward the plasma membrane (Bose *et al.*, 2002). In peripheral regions there is a higher percentage of plus ends facing outward so a plus-end–directed myosin would be appropriate for vesicle trafficking outward for exocytosis. As a minus-end–directed motor, myo6 is suited to play the opposite role, moving uncoated vesicles inward away from the plasma membrane for fusion with the early endosome.

The uncoated vesicles analyzed in our time-lapse studies took a circuitous route to exit the actin-rich periphery. They did not appear to move along one specific actin track to exit the actin mesh nor did the vesicles in each area appear to have preset endosomal destinations. Instead, the uncoated vesicles apparently switched between actin tracks. This type of motility is consistent with the kinetic analysis of myo6 movement in vitro, which predicted short processive runs interspersed with pauses (Rock *et al.*, 2001) and also with modeling of motor-assisted transport of particles in situations of mixed filament polarities and a minus-end–directed motor (Smith and Simmons, 2001). Because actin at the plasma membrane is biased with minus-ends inward, this start-and-stop motility by myo6 would eventually lead to vesicle exit from the actin mesh. Therefore, actin is a barrier to vesicle trafficking, but myo6 as a minus-end–directed motor takes advantage of the features of this barrier to transport uncoated vesicles to the early endosome for fusion.

ACKNOWLEDGMENTS

We thank the Michael David lab for use of their plate reader. We recognize the efforts of Dawn Jolson and Jennifer Stubbs, who worked to perfect the ELISA assay used to quantify transferrin uptake. We thank Ryan Littlefield for providing an Excel spreadsheet for calculating vesicle MSDs. This work was supported by Research Grant 6-FY02–150 and a Basil O'Connor Starter Scholar Research Grant from the March of Dimes Birth Defects Foundation and a grant from the National Institutes of Health (R01-EY12695) to T.H.

REFERENCES

Abney, J.R., Meliza, C.D., Cutler, B., Kingma, M., Lochner, J.E., and Scalettar, B.A. (1999). Real-time imaging of the dynamics of secretory granules in growth cones. Biophys. J. *77,* 2887–2895.

Aschenbrenner, L., Lee, T., and Hasson, T. (2003). Myo6 facilitates the translocation of endocytic vesicles from cell peripheries. Mol. Biol. Cell *14,* 2728–2743.

Bose, A., Guilherme, A., Robida, S.I., Nicoloro, S.M.C., Zhou, Q.L., Jiang, Z.Y., Pomerleau, D.P., and Czech, M.P. (2002). Glucose transporter recycling in response to insulin is facilitated by mysoin Myo1c. Nature *420,* 821–824.

Clague, M.J. (1998). Molecular aspects of the endocytic pathway. Biochem. J. *336,* 271–282.

Cramer, L.P. (1997). Molecular mechanism of actin-dependent retrograde flow in lamellipodia of motile cells. Front. Biosci. *2,* d260–d270.

De Vries, L., Lou, X., Zhao, G., Zheng, B., and Farquhar, M.G. (1998). GIPC, a PDZ domain containing protein, interacts specifically with the C terminus of RGS-GAIP. Proc. Natl. Acad. Sci. USA *95,* 12340–12345.

Dunn, K.C., Aotaki-Keen, A.E., Putkey, F.R., and Hjelmeland, L.M. (1996). ARPE-19, a human retinal pigment epithelial cell line with differentiated properties. Exp. Eye Res. *62,* 155–169.

Eitzen, G. (2003). Actin remodeling to facilitate membrane fusion. Biochim. Biophys. Acta *1641,* 175–181.

Eskelinen, S., Kok, J.W., Sormunen, R., and Hoekstra, D. (1991). Coated endosomal vesicles: sorting and recycling compartment for transferrin in BHK cells. Eur. J. Cell Biol. *56,* 210–222.

Goodson, H.V., Valetti, C., and Kreis, T.E. (1997). Motors and membrane traffic. Curr. Opin. Cell Biol. *9,* 18–28.

Gorvel, J.P., Chavrier, P., Zerial, M., and Gruenberg, J. (1991). rab5 controls early endosome fusion in vitro. Cell *64,* 915–925.

Gruenberg, J. (2001). The endocytic pathways: a mosaic of domains. Nat. Rev. Mol. Cell. Biol. *2,* 721–730.

Hanover, J.A., Willingham, M.C., and Pastan, I. (1984). Kinetics of transit of transferrin and epidermal growth factor through clathrin-coated membranes. Cell *39,* 283–293.

Hasson, T. (2003). Myosin VI: two distinct roles in endocytosis. J. Cell Sci. *116,* 3453–3461.

Hasson, T., and Mooseker, M.S. (1994). Porcine myosin-VI: characterization of a new mammalian unconventional myosin. J. Cell Biol. *127,* 425–440.

Homma, K., Yoshimura, M., Saito, J., Ikebe, R., and Ikebe, M. (2001). The core of the motor domain determines the direction of myosin movement. Nature *412,* 831–834.

Hopkins, C.R. (1983). Intracellular routing of transferrin and transferrin receptors in epidermoid carcinoma A431 cells. Cell *35,* 321–330.

Liu, T.F., Kandala, G., and Setaluri, V. (2001). PDZ-domain protein GIPC interacts with the cytoplasmic tail of melanosomal membrane protein gp75 (tyrosinase related protein-1). J. Biol. Chem. *276,* 35768–35777.

Mukherjee, S., Ghosh, R.N., and Maxfield, F.R. (1997). Endocytosis. Physiol. Rev. *77,* 759–803.

Nielsen, E., Severin, F., Backer, J.M., Hyman, A.A., and Zerial, M. (1999). Rab5 regulates motility of early endosomes on microtubules. Nat. Cell Biol. *1,* 376–382.

Oheim, M., and Stuhmer, W. (2000). Tracking chromaffin granules on their way through the actin cortex. Eur. Biophys. J. *29,* 67–89.

Pfeffer, S.R., Dirac, S.A., and Soldati, T. (1995). Rab GDI dissociation inhibitor, putting GTPases in their right place. J. Biol. Chem. *270,* 17057–17059.

Qualmann, B., and Kessels, M.M. (2002). Endocytosis and the cytoskeleton. Int. Rev. Cytol. *220,* 93–144.

Qualmann, B., Kessels, M.M., and Kelly, R.B. (2000). Molecular links between endocytosis and the actin cytoskeleton. J. Cell Biol. *150,* F111–F116.

Rock, R.S., Rice, S.E., Wells, A.L., Purcell, T.J., Spudich, J.A., and Sweeney, H.L. (2001). Myosin VI is a processive motor with a large step size. Proc. Natl. Acad. Sci. USA *98,* 13655–13659.

Rose, S.D., Lejen, T., Casaletti, L., Larson, R.E., Dumitrescu Pene, T., and Trifaro, J.-M. (2002). Molecular motors involved in chromaffin cell secretion. Ann. NY Acad. Sci. *971,* 222–231.

Rudolf, R., Kogel, T., Kuznetsov, S.A., Salm, T., Schlicker, O., Hellwig, A., Hammer, J.A., III, and Gerdes, H.-H. (2002). Myosin Va facilitates the distribution of secretory granules in the F-actin rich cortex of PC12 cells. J. Cell Sci. *116,* 1339–1348.

Ruppel, K.M., and Spudich, J.A. (1996). Structure-function analysis of the motor domain of myosin. Annu. Rev. Cell Dev. Biol. *12,* 543–573.

Sankaranarayanan, S., Atluri, P.P., and Ryan, T.A. (2003). Actin has a molecular scaffolding, not propulsive, role in presynaptic function. Nat. Neurosci. *6,* 127–135.

Schmid, S.L. (1997). Clathrin-coated vesicle formation and protein sorting: an integrated process. Annu. Rev. Biochem. *66,* 511–548.

Smith, D.A., and Simmons, R.M. (2001). Models of motor-assisted transport of intracellular particles. Biophys. J. *80,* 45–68.

Smythe, E., Redelmeier, T.E., and Schmid, S.L. (1992). Receptor-mediated endocytosis in semi-intact cells. Methods Enzymol. *219,* 223–234.

Spector, I., Shochet, N.R., Kashman, Y., and Groweiss, A. (1983). Latrunculins: novel marine toxins that disrupt microfilament organization in cultured cells. Science *219,* 493–195.

Trischler, M., Stoorvogel, W., and Ullrich, O. (1999). Biochemical analysis of distinct rab5- and rab11-positive endosomes along the transferrin pathway. J. Cell Sci. *112,* 4773–4783.

Wells, A.L., Lin, A.W., Chen, L.-Q., Safer, D., Cain, S.M., Hasson, T., Carragher, B.O., Milligan, R.A., and Sweeney, H.L. (1999). Myosin VI is a myosin that moves backwards. Nature *401,* 505–508.

Yoshimura, M., Homma, K., Saito, J., Inoue, A., Ikebe, R., and Ikebe, M. (2001). Dual regulation of mammalian myosin VI motor function. J. Biol. Chem. *276,* 39600–39607.

Zerial, M., and McBride, H. (2001). Rab proteins as membrane organizers. Nature Rev. Mol. Cell. Biol. *2,* 107–119.